

Near- Θ Polymers in a Cylindrical Space

Youngkyun Jung,* Changbong Hyeon,* and Bae-Yeun Ha*

Cite This: *Macromolecules* 2020, 53, 2412–2419

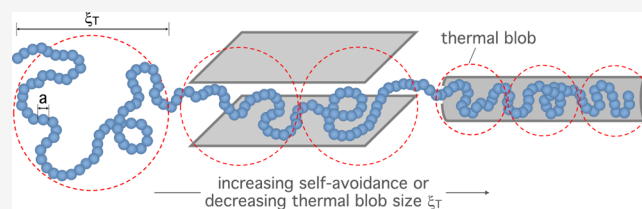
Read Online

ACCESS |

Metrics & More

Article Recommendations

ABSTRACT: The advent of single-molecule manipulations has renewed our interest in understanding chain molecules in confined spaces. The conformation and dynamics of these molecules depend on the degree of confinement and self-avoidance. A distinguishing feature of weakly self-avoiding polymers (e.g., DNA) in a cylindrical space is the emergence of the so-called extended de Gennes regime. On the other hand, an earlier study indicates that slit confinement enhances the self-avoidance of a Θ -polymer, for which the two-body (monomer–monomer) interaction vanishes. Using molecular dynamics simulations, we study how cylindrical confinement modulates the self-avoidance of near- Θ polymers. Our results suggest that the confinement enhances self-avoidance, turning a near- Θ solvent into a good solvent. This finding has a number of nontrivial consequences. First, it induces the linear ordering of a near- Θ chain, as if the chain is in a good solvent. Second, under strong confinement, the chain size, $R_{||}$, scales with the cylinder diameter, D , approximately as $R_{||} \approx Na(D/a - 1)^{-4/3}$, where N is the number of monomers and a the monomer size. This is distinct from $R_{||} \approx Na(D/a)^{-1}$ as suggested by the conventional picture, in which the second virial coefficient, B_2 , remains unchanged upon confinement. In contrast, enhanced self-avoidance is not easily felt by the confinement free energy unless B_2 is large enough, outside the regime of a near- Θ solvent. Finally, we show how these findings are related to long-range bond–bond correlations observed for single polymers or polymer melts.



INTRODUCTION

The thermodynamic properties of polymer solutions are dictated by monomer–monomer, monomer–solvent, and solvent–solvent interactions.^{1,2} In the Flory–Huggins approach, these interactions as well as the entropy of mixing are subsumed into the (effective) monomer–monomer interaction parameter, ν . The value of ν is controlled by the quality of the solvent and is related to the second virial coefficient of monomers B_2 as $\nu = 2B_2$.² In a strict- Θ solvent, ν vanishes; higher-order interactions give rise to a logarithmic correction to chain sizes.^{3,4} More practically, in a near- Θ solvent, $\nu \approx 0$. In this case, the notion of thermal blobs is useful:¹ inside a thermal blob, self-avoidance is insignificant (see Figure 1, where the thermal blob is represented by the dashed circles in red). For a near- Θ chain, the thermal blob size is much larger than the monomer size or even comparable to the chain size: $\xi_T \approx R_g$, where R_g stands for the radius of gyration. If a is the size of each monomer, the thermal blob size is given by $\xi_T \approx a^4/|\nu| = a^4/2|B_2|$ ($\approx a$ in an athermal solvent).¹

In a conventional picture, ν depends on the temperature, but its dependence on other external parameters, such as confinement, has often been under-appreciated.^{1,5} A recent study, however, suggests that the second virial coefficient of a Θ polymer becomes positive in a slit confinement.⁴

Beyond this effort,⁴ the interplay between the self-avoidance of polymers and external constraints remains to be further explored considering the recent booming interest in cylindrically

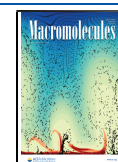
confined polymers.^{6–12} Indeed, it will be instructive to test conventional approaches against simulation data for near- Θ polymers in a cylindrical space. Under the right conditions, they fall in the extended de Gennes regime.^{6–10} In the literature, semiflexible chains (e.g., DNA) were considered, since their excluded volume interactions are weak.^{6–9} This regime has not been characterized for flexible polymers near the Θ point. Is the extended de Gennes regime also realized for these flexible polymers with weak self-avoidance or at $T \approx \Theta$? How sensitively does their self-avoidance depend on the degree of confinement?

Here, we study how cylindrical confinement modulates the self-avoidance of a polymer, as measured by the value of B_2 or ν , and its consequences on the way the polymer behaves. To this end, we use molecular dynamics (MD) simulations. We start with a polymer in a near- Θ solvent in the bulk and confine it in a cylindrical space. The effect of confinement is twofold. Obviously, it reduces the conformational space of the polymer by limiting allowed conformations.^{1,10} Also, confinement modulates self-avoidance, as if it lowered the Flory temperature Θ , turning the near- Θ solvent into a good solvent. This is well

Received: November 10, 2019

Revised: February 28, 2020

Published: March 18, 2020



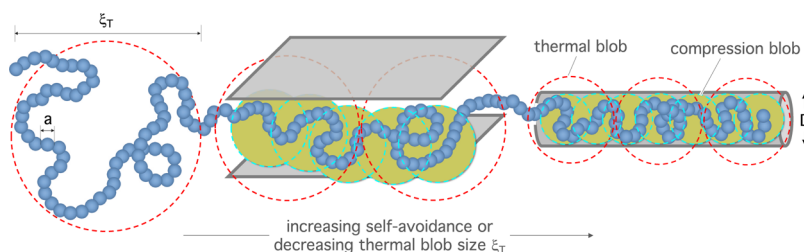


Figure 1. Confined spaces and self-avoidance. Physical confinement influences the spatial organization of a polymer. First, it reduces the conformational space of the polymer by limiting allowed conformations. Second, it modulates self-avoidance.⁴ If the polymer chain is in a near- Θ solvent in the bulk, self-avoidance is negligible (Figure 2). The thermal blob size is comparable to the chain size: $\xi_T \approx a^4/|v| \approx 2R_g$. The dashed circles in red represent the thermal blob, inside which self-avoidance is insignificant. Confinement increases self-avoidance, as if it changes the solvent quality, turning the near- Θ solvent into a good solvent, as detailed in Figures 3–5 (see ref 4 for the slit confinement). The stronger the confinement is, the stronger the self-avoidance is and the smaller the thermal blob size ξ_T is. The dashed circles of size D each in cyan represent free-energy units: $k_B T$ per each unit. Note that they tend to overlap each other when self-avoidance is weak. As self-avoidance becomes strong, the degree of overlapping is diminished while ξ_T tends to D , the size of the free-energy unit.

aligned with the slit-confined case.⁴ The stronger the confinement is, the stronger the self-avoidance is and the smaller the thermal blob size ξ_T is, as illustrated in Figure 1.

Confinement-enhanced self-avoidance has a number of non-trivial consequences. First, it induces the linear ordering of a near- Θ chain, which would remain randomly organized in the bulk. It is worth noting that three-body interactions become important in a cylindrical space (or in lower dimensions) and can in principle induce the linear ordering of a Θ polymer.⁵ A hidden assumption in this picture is that ν is independent of confinement. As evidenced below and as noted earlier,⁴ $\nu = 2B_2$ changes with the degree of confinement. As a result, the expected D -dependence of chain sizes from a conventional picture,⁵ in which B_2 remains unchanged upon confinement, is not realized. Our results suggest that in the limit $N \rightarrow \infty$, the chain size, $R_{||}$, scales with the cylinder diameter, D , as $R_{||} \approx Na(D/a - 1)^{-4/3}$, where N is the number of monomers and a the monomer size, not as $Na(D/a)^{-1}$ as suggested by ref 5.

In contrast, enhanced self-avoidance is not easily felt by the confinement free energy unless the second virial coefficient is large enough, possibly outside a near- Θ solvent. This seeming contradiction can be resolved by contrasting compression blobs with thermal blobs.^{1,10} The former can be viewed as a free-energy unit: a free-energy cost of $k_B T$ per compression blob. When the compression blob is smaller than the thermal blob, the confinement free-energy scales linearly with the number of compression blobs, independent of the degree of self-avoidance.

Finally, we relate our results to the earlier finding that chain connectivity gives rise to long-range bond–bond correlations along a linear chain under a variety of conditions (e.g., in a melt, in a near- Θ solvent, and under tube confinement). Indeed, enhanced self-avoidance is well manifested in the bond–bond correlations. This results in correlations longer ranged than expected for a Θ chain.

SIMULATION PROCEDURE

Our MD simulations are based on the bead-spring model of a polymer chain: beads or monomers of size a each. If r is the center-to-center distance between beads, adjacent beads are connected to each other through the finitely extensible nonlinear elastic (FENE) potential

$$U_{\text{FENE}}(r) = -\frac{1}{2}kr_0^2 \ln \left[1 - \left(\frac{r}{r_0} \right)^2 \right] \quad (1)$$

where the spring constant, k , and the range of $U_{\text{FENE}}(r)$ are set to $k = 30.0\epsilon/a$ and $r_0 = 1.5a$.^{13,14} The beads interact with each other through a truncated-shifted Lennard-Jones (LJ) potential given by^{15,16}

$$U(r) = \begin{cases} U_{\text{LJ}}(r) - U_{\text{LJ}}(r_c) & \text{for } r < r_c \\ 0 & \text{otherwise} \end{cases} \quad (2)$$

where $U_{\text{LJ}}(r)$ is the conventional LJ potential

$$U_{\text{LJ}}(r) = 4\epsilon \left[\left(\frac{\sigma}{r} \right)^{12} - \left(\frac{\sigma}{r} \right)^6 \right] \quad (3)$$

where ϵ and σ represent the strength and range of the LJ potential, respectively. The parameter σ can be designated as the size of each bead or monomer.

The polymer chain is trapped inside a cylindrical space, made of “imaginary” beads of size a each, interacting with polymer beads through $U(r)$ in eq 2 with $r_c = 2^{1/6}a$. When a particle approaches the wall, it interacts with an “image” particle; it undergoes a head-on collision with the image particle.²⁴

The equation of motion for beads is integrated using the velocity-Verlet algorithm with a time step 0.01τ , where $\tau = a\sqrt{m/\epsilon}$ (m is the bead mass), while the system is kept at a constant temperature, $T = 1.0\epsilon/k_B$, via a Langevin thermostat with a damping constant, $\gamma = 1.0\tau^{-1}$.¹⁴ Here, k_B is the Boltzmann constant. For our simulations, we used the simulation package LAMMPS (“large-scale atomic/molecular massively parallel simulator”).¹⁷

We prepare polymer chains near the Θ point by adjusting the value of r_c . Recall that the second virial coefficient B_2 is given by

$$B_2(T) = \frac{1}{2} \int_0^{r_c} (1 - e^{-U(r)/k_B T}) d^3r \quad (4)$$

Also note that the excluded volume of monomers, ν , is related to B_2 via $\nu = 2B_2$. The value of B_2 can be adjusted by changing the value of r_c . Here, we mainly choose $r_c = 1.4912a, 1.4915a$, unless otherwise stated, corresponding to $B_2 \approx 0.00202a^3, -0.00047a^3$, respectively.

After equilibration for about 10^8 time steps, we performed a simulation run for 3×10^9 time steps and obtained data every 2×10^4 time steps; the chain relaxation time obtained from the autocorrelation function of the farthestmost distance of a confined chain $R_{||}$ was found to be $\approx 10^7$ time steps for $N = 3000$, which is the largest value of N used in this work.

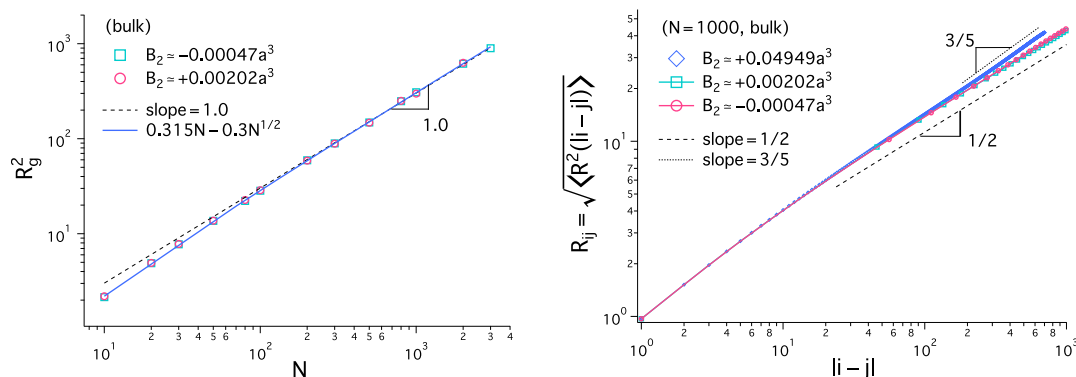


Figure 2. (Left) Square radius of gyration in the bulk R_g vs N , the number of monomers. For small second virial coefficients, $B_2 \approx -0.00047a^3$ (corresponding to $r_c = 1.4915a$ in eq 2) and $+0.00202a^3$ ($r_c = 1.4912a$), the chain behaves as an ideal chain characterized by $R_g^2 \approx N^{2\nu}$ ($\nu = 1/2$), as long as $200 < N \lesssim 3000$. For $N < 200$, the N dependence of R_g^2 deviates from the ideal chain behavior. Indeed, the blue curve, representing eq 5, fits the data well for the entire N range shown. For short length scales, bond–bond correlations due to chain connectivity (the second term in eq 5) can cause chain statistics to deviate from ideality.¹⁹ For sufficiently large $N \gg 3000$, the scaling exponent will eventually become $\nu = 3/5$ for $B_2 > 0$ or $\nu = 1/3$ for $B_2 < 0$, as expected from the picture of a polymer in a good and poor solvent, respectively. (Right) Internal distance of a chain in the bulk $R_{ij} = \langle R^2(li - jl) \rangle^{1/2}$ for $N = 1000$ and for $B_2 = -0.00047a^3$, $0.00202a^3$, $0.04949a^3$. When $B_2 = -0.00047a^3$, $0.00202a^3$, the polymer behaves as an ideal chain if $li - jl \gtrsim 200$. For large $B_2 = 0.04949a^3$, the chain shows self-avoiding chain statistics, that is, $\nu = 3/5$, as long as $li - jl > 100$. For sufficiently small $li - jl$, the bond–bond correlations observed in the left graph dominate the behavior of R_{ij} .

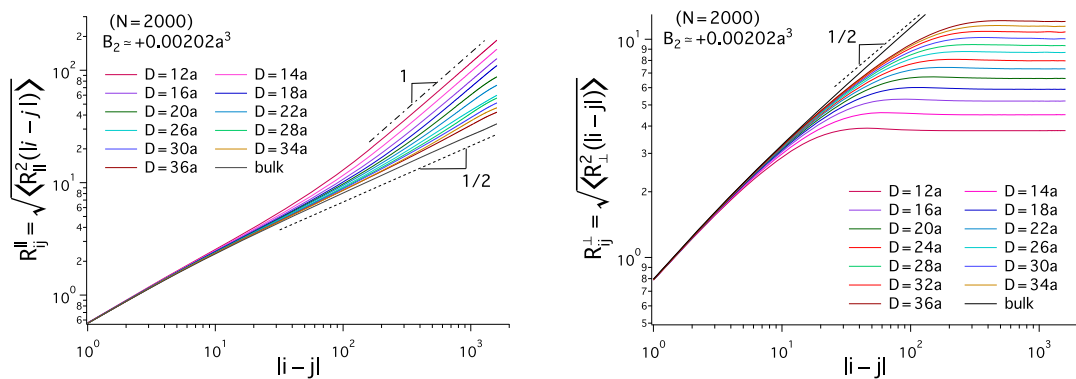


Figure 3. Internal distance of a polymer in a cylinder of diameter D : longitudinal (left) and transverse component (right). We have chosen $B_2 \approx 0.00202a^3$ and $N = 2000$ and used various values of $D = 12a, 14a, \dots, 36a, \infty$, represented by curves in various colors. (Left) This graph shows the longitudinal internal distance, $R_{ij}^{\parallel} = \langle R_{\parallel}^2(li - jl) \rangle^{1/2}$, where $R_{\parallel}(li - jl)$ is the longitudinal component of $\mathbf{R}(li - jl)$. In the bulk ($D = \infty$), the ideal-chain statistics governs the longitudinal internal distance for a large $li - jl$ range: $R_{ij}^{\parallel} \approx li - jl^{1/2}$ (black dashed line). We expect this ideal-chain behavior to persist unless $D < 2R_g$. Indeed, as D decreases, the slope starts to deviate from that of an ideal chain, that is, $1/2$, and increases up to 1. The slope of the internal distance is set by the extent of confinement. As $li - jl$ becomes large, the internal distance approaches the polymer size. The slope 1 signals the linear ordering of the chain in a cylindrical confinement. (Right) This graph shows the transverse component of the internal distance of a chain, $R_{ij}^{\perp} = \langle R_{\perp}^2(li - jl) \rangle^{1/2}$. For the entire range of D used ($D = 12a, 14a, \dots, 36a$), the ideal-chain regime is captured by R_{ij}^{\perp} ; the self-avoiding regime is absent. This is correlated with the finding that the crossover of R_{ij}^{\parallel} from the ideal-chain to the self-avoiding chain occurs for a large value of $li - jl$, as shown in the left graph. The strongly confined (linearly organized) chain is thus in the extended de Gennes regime. Also, it is well aligned with the confinement free energy of a Θ chain ($\mathcal{F}_{\text{conf}} \approx D^{-2}$), suggested by the results for the force exerted by the chain on the inner wall of a cylinder (i.e., $f \approx D^{-3}$) in Figure 4.

RESULTS AND DISCUSSION

We have first characterized chain conformations in a free space. Figure 2 displays our results for chain sizes (left) and internal distances (right). In this work, N is the number of monomers and a the size of each monomer. In the bulk, the radius of gyration, R_g , proves to be a convenient choice for the chain size.² Let $\langle \dots \rangle$ be an ensemble average of \dots . The radius of gyration is given by $R_g^2 = \frac{1}{2N^2} \sum_{i,j=1}^N \langle (\mathbf{r}_i - \mathbf{r}_j)^2 \rangle$; the internal distance, R_{ij} , between monomers i and j is defined as $R_{ij} = \langle R^2(li - jl) \rangle^{1/2}$.

In the graph on the left in Figure 2, the square radius of gyration in the bulk R_g is plotted as a function of the number of monomers, N , for a few choices of B_2 . Here and below, B_2 refers to the bulk; the corresponding quantity under the cylindrical confinement will be denoted as B_2^{cyl} . For small second virial

coefficients, as required for a near- Θ solvent, that is, $B_2 \approx -0.00047a^3$ (corresponding to $r_c = 1.4915a$ in eq 2) and $+0.00202a^3$ ($r_c = 1.4912a$), the chain behaves as an ideal chain characterized by $R_g^2 \approx N^{2\nu}$ with $\nu = 1/2$, as long as $200 < N \lesssim 3000$. In three dimensions, higher-order terms (e.g., three-body interactions) have a minimal effect on chain sizes.^{3,4} A polymer in a near- Θ solvent is thus expected to behave as an ideal chain. This is well aligned with the observed scaling exponent of R_g^2 .

For $N < 200$, however, the N dependence of R_g^2 deviates from the ideal chain behavior. This can be understood in terms of long-range bond–bond correlations due to chain connectivity.¹⁹ As a result, the size of a Θ or near- Θ polymer chain ($R_g \lesssim \xi_T$) is given by

$$\langle R_g^2 \rangle \approx \alpha N + \beta N^{1/2} \quad (5)$$

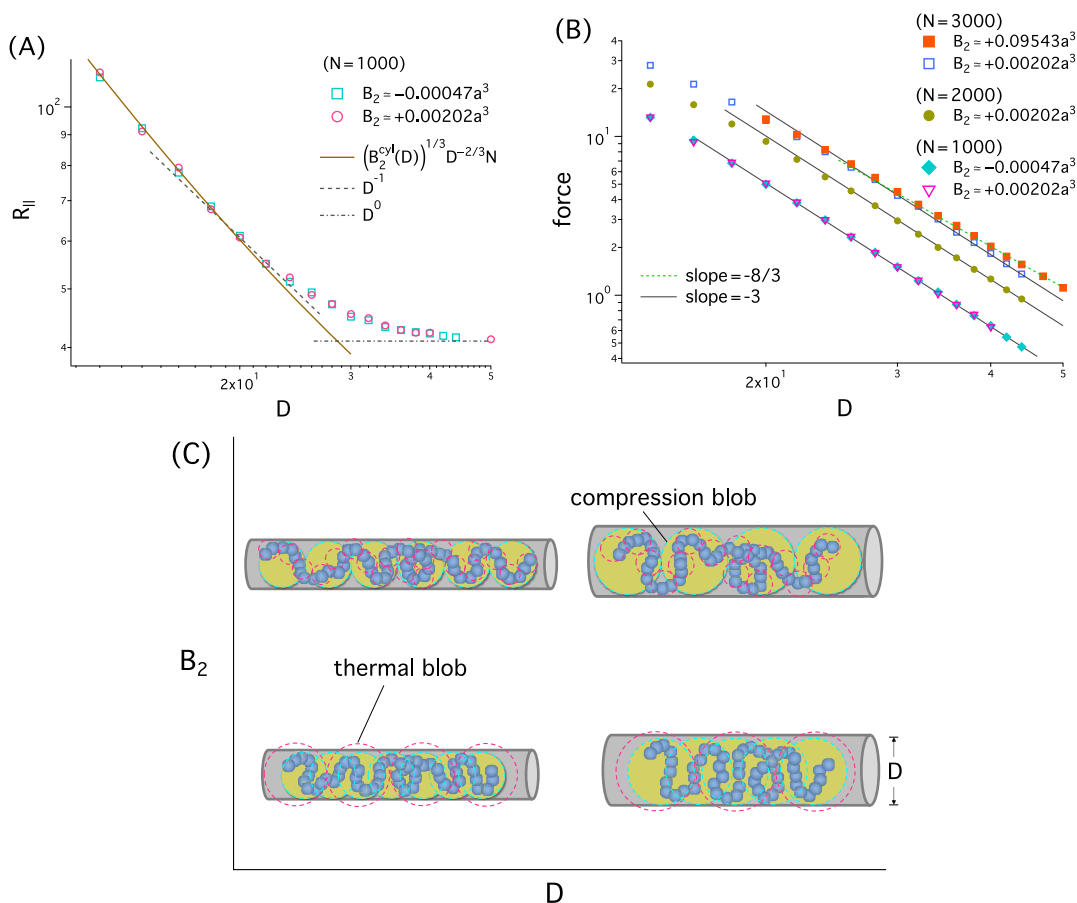


Figure 4. (A) Chain size (farthestmost distance) of a cylindrically confined polymer as a function of D . We have chosen $B_2 \approx -0.00047a^3, 0.00202a^3$ and $N = 1000$. The solid line in brown is the best fit to the simulation data, described by $R_{||} \approx Na(D/a - 1)^{-4/3} + \text{const.}$ (or $R_{||} \approx Na(D/a - 1)^{-4/3}$ in the limit $N \rightarrow \infty$). This deviates from the earlier result, $R_{||} \approx Na(D/a)^{-1}$, described by the dashed line, in which three-body repulsions extend the chain,⁵ as well as from what we expect from an ideal chain (the dot-dashed line). The discrepancy between the solid and dotted lines can be attributed to confinement effects: $B_2^{\text{eff}} > 0$, when $B_2 \approx 0$. (B) Force (f) exerted by the confined chain on the curved wall of a cylinder as a function of D for several values of B_2 and for $N = 1000, 2000, 3000$. For $D \gtrsim 20a$, $f(D) \approx D^{-3}$, which is consistent with the confinement free energy of a Θ chain: $\mathcal{F}_{\text{conf}}(D) \approx D^{-2}$. This is well aligned with the notion of compression blobs of size D each as free-energy units: $k_B T$ per compression blob. As long as $D < \xi_T$, the neighboring compression blobs overlap each other. For large $B_2 \approx 0.09543a^3$, $\xi_T \approx 5 \lesssim D$ (in the D range shown in the graph). As a result, self-avoiding statistics is manifested in the force– D relation: $f(D) \approx D^{-8/3}$ [$\mathcal{F}_{\text{conf}}(D) \approx D^{-5/3}$]. (C) Diagram showing the organization of a confined polymer in a $D-B_2$ plane. The confined chain can be viewed as a linear succession of possibly overlapping compression blobs of size $\approx D$ each, represented by circles in cyan. The degree of overlapping between compression blobs is set by the size of the thermal blob ξ_T represented by circles in red; recall $\xi_T = a^4/v \approx a/(1 - \Theta/T)$, where v is the excluded volume. The larger D/ξ_T is, the more strongly they repel each other, as is the case for larger B_2 . For sufficiently large D/ξ_T , the compression blobs become linearly arranged without overlapping. Also note that for the same B_2 , ξ_T is smaller for smaller D . The lower two cylinders represent the extended de Gennes regime; the upper two belong to the de Gennes regime.

Besides the obvious (i.e., ideal-chain-like) first term, the second term arises from chain connectivity, which is responsible for the deviation of Θ chains from ideality.¹⁹ We expect this to be relevant for near- Θ chains in Figure 2. This is indeed the case: this relation, represented by the blue solid curve, fits the data well for the entire N range shown. For a small N range, the \sqrt{N} dependence, arising from the connectivity-induced bond–bond correlation, is dominant.

For a sufficiently large $N \gg 3000$, one can legitimately argue that the scaling exponent will eventually become $\nu = 3/5$ ($\equiv \nu_F$, the Flory exponent) for $B_2 > 0$ or $\nu = 1/3$ for $B_2 < 0$, as expected from the picture of a polymer in a good and poor solvent, respectively.¹ The concept of thermal blobs proves to be useful in this consideration. Inside each blob of size ξ_T , the chain statistics resembles that of an ideal chain. For small ν as in a near- Θ solvent, $\xi_T \approx a^4/|v|$ can be as big as R_g for some range of N . Beyond a certain value of N , denoted as $N_T \approx (\xi_T/a)^2$, R_g

becomes larger than ξ_T . If so, the interaction between monomers will swell or collapse the polymer, depending on the sign of B_2 . For $B_2 \approx 0.00202a^3$, $\xi_T \approx 250a$. The corresponding N value (N_T) is $N_T \approx 250^2 \approx 60,000$, which is prohibitively long to be considered in simulations.

The graph on the right in Figure 2 summarizes our results for the internal distance of a polymer chain in the bulk, $R_{ij} = \langle \mathbf{R}^2(li - jl) \rangle^{1/2}$, for $N = 1000$; we have used the following choices of B_2 : $B_2 \approx -0.00047a^3, 0.00202a^3, 0.04949a^3$. When $B_2 \approx -0.00047a^3, 0.00202a^3$, as in the left graph, the polymer behaves as an ideal chain as long as $li - jl > 200$. For large $B_2 \approx 0.04949a^3$ ($N_T \approx 100$), the chain shows self-avoiding chain statistics, $\nu = 3/5$, if $li - jl > N_T$. For sufficiently small $li - jl$, the chain statistics should reflect the long-range bond–bond correlations, similar to what is observed in the left graph.

We have then trapped a near- Θ polymer chain in a cylindrical space of diameter D and examined chain conformations.

Because of the anisotropic confinement, it proves useful to decompose the internal distance in the longitudinal and transverse direction: $R_{ij}^{\parallel} = \langle R_{\parallel}^2(li - jl) \rangle^{1/2}$ and $R_{ij}^{\perp} = \langle R_{\perp}^2(li - jl) \rangle^{1/2}$.

Figure 3 displays our results for R_{ij}^{\parallel} (left) and R_{ij}^{\perp} (right) in a log–log plot. We have chosen $B_2 \approx 0.00202a^3$ and $N = 2000$ and used several values of $D = 12a, 14a, \dots, 36a, \infty$, represented by lines in various colors. In the bulk ($D = \infty$), the radius of gyration is estimated to be $R_g \approx 25a$; also, the ideal-chain statistics governs the longitudinal internal distance except for a small $li - jl$ range, similar to what is observed in the bulk case in Figure 2: $R_{ij}^{\parallel} \approx li - jl^{1/2}$ (black line); the slope of a curve in this log–log graph coincides with the exponent of R_{ij} . We expect this bulk behavior to persist unless $D < 2R_g = 2 \times 25a$. As D decreases, the slope starts to deviate from that of an ideal chain, $1/2$, and increases up to 1. The slope of the internal distance is set by the degree of confinement. The slope 1 signals the linear ordering of the chain in a cylindrical confinement.^{6–10}

The gradual increase of the slope of the curves with decreasing D in the R_{ij}^{\parallel} graph in Figure 3, from the slope of an ideal chain to that of a linearly organized chain, tends to point to the significance of confinement in enhancing self-avoidance, as in slit geometry.⁴ While three-body interactions can induce linear ordering in a cylindrical space, below we present evidence that this arises from two-body interactions.

The graph on the right in Figure 3 shows the transverse component of the internal distance of a chain, $R_{ij}^{\perp} = \langle R_{\perp}^2(li - jl) \rangle^{1/2}$, for $B_2 \approx 0.00202a^3$ and for $N = 2000$. For the entire range of D used ($D = 12a, 14a, \dots, 36a$), the ideal-chain regime is captured by R_{ij}^{\perp} , but the self-avoiding regime characterized by the slope $\nu = 3/5$ (often designated as the Flory exponent ν_F^{-1}) is not realized. This is correlated with the finding that the crossover of R_{ij}^{\parallel} from the ideal-chain to the linearly organized regime occurs for large $li - jl$, as shown in the graph on the left.

The confined chain presented in Figure 3 thus falls in the extended de Gennes regime,^{6–10} as is most obvious for a small- D range. As illustrated on the right in Figure 1, a weakly self-avoiding chain in a cylinder can be viewed as a linear succession of possibly overlapping compression blobs of size D each. For large D (e.g., $D = 34a, 36a$), however, the effect of confinement is marginal and the linear regime is not realized with the choice $N = 2000$. But for sufficiently large N , the chain will eventually enter this regime. The small- D case presented here is well aligned with the confinement free energy of a Θ chain ($\mathcal{F}_{\text{conf}} \approx D^{-2}$), suggested by the results for the force exerted by the chain on the inner wall of a cylinder (i.e., $f \approx D^{-3}$) in Figure 4B.

In order to gain further insights into the confinement-induced self-avoidance, we have considered the D -dependence of chain sizes as well as that of the force exerted by monomers on the cylinder wall. Here, the chain size is taken to be the farthest distance of the chain in the longitudinal direction, denoted as R_{ij} .¹⁰ This consideration will further clarify how confinement modulates the self-avoidance of a cylindrically confined polymer.

The graph in Figure 4A shows our results for R_{ij} versus D . For this, we have chosen $B_2 \approx -0.00047a^3, 0.00202a^3$ and $N = 1000$, as in Figure 2. Even though the corresponding unconfined polymer chain behaves like an ideal chain, as shown in Figure 2, the results in this figure suggest that the chain size increases with a decreasing pore diameter, D . This means that confinement stretches an otherwise Θ chain along the long axis of the cylinder, as suggested in Figure 3. In an earlier approach,⁵ this

was attributed to three-body repulsions. When $B_2 = 0$, the Flory free energy of a cylindrically confined Θ chain is given by

$$\frac{F_{\text{Flory}}}{k_B T} \approx \frac{R_{\parallel}^2}{Na^2} + \frac{B_3}{3!} \frac{N^3}{(R_{\parallel} D^2)^2} \quad (6)$$

where B_3 is the third virial coefficient. This equation leads to $R_{\parallel} \approx Na(D/a)^{-1}$. However, this scaling relation described by the dashed line in Figure 4A deviates from the data. The discrepancy between the solid and dotted lines can be attributed to confinement effects: cylindrical confinement turns $B_2 = 0$ into $B_2^{\text{cyl}} > 0$ (recall that B_2^{cyl} is the second virial coefficient in the cylindrical geometry).

Does the confinement effect on B_2 alone account for the data? To answer this question, we have examined the confinement-enhanced second virial coefficient, $B_2^{\text{cyl}}(D)$, which is generally different from B_2 in the bulk. For $D > 2a$, it can be approximated as $B_2^{\text{cyl}}(D) \approx a^3(D/a)^2/(D/a - 1)^4$ (see the Appendix). Up to two-body interactions, the Flory free energy is given by

$$\frac{F_{\text{Flory}}}{k_B T} \approx \frac{R_{\parallel}^2}{Na^2} + \frac{B_2^{\text{cyl}}(D)}{2} \frac{N^2}{R_{\parallel} D^2} \quad (7)$$

Earlier, a renormalized Flory approach was used for a cylindrically confined polymer with self-avoidance.¹⁸ As far as chain sizes are concerned, eq 7 serves its purpose well. The minimization of this free energy with this choice of B_2^{cyl} leads to

$$R_{\parallel} \approx N(B_2^{\text{cyl}}(D))^{1/3}(D/a)^{-2/3} + \text{const.} \\ \approx Na(D/a - 1)^{-4/3} + \text{const.} \quad (8)$$

where the constant term is introduced to ensure a crossover from the linearly organized to the D -independent bulk behavior. In the large- N limit, the constant term becomes irrelevant. The solid line in brown in Figure 4A is the best fit of this to the simulation data. For $D \lesssim 20a$, the agreement between the solid line and the data is excellent; for a larger value of D , however, the effect of confinement is marginal or insignificant. This agreement suggests that upon confinement, a Θ chain evolves into a self-avoiding one, which tends to become linearly organized.

In the graph in Figure 4B, the force (f) exerted by the confined chain on the curved wall of a cylinder is shown as a function of D for several small values of B_2 and for $N = 1000, 2000, 3000$. For $D \gtrsim 20a$, $f(D) \approx D^{-3}$, which is consistent with the confinement free energy of a Θ chain: $\mathcal{F}(D) \approx D^{-2}$. This seems to contradict the physical picture captured in Figure 3 as well as in the graph in Figure 4A: turning a near- Θ solvent to a good solvent. This seeming contradiction can be resolved in terms of what is referred to as a “free-energy unit” (the dashed circles in cyan in Figure 1) versus the thermal blob (the dashed circle in red). The free-energy unit coincides with the compression blob. The free-energy unit of size D describes the free-energy cost for confinement: $\sim k_B T$ per each unit. In a random walk analogy, each time the random walk travels a distance D , as described by the cyan circle, and collides with the cylinder wall, its direction changes. This reasoning leads to $k_B T$ per each unit. As long as $D < \xi_T$, the neighboring free-energy units overlap each other.

In contrast, for large $B_2 \approx 0.09543a^3$, $\xi_T \approx 5a \lesssim D$ unless D is sufficiently small. As a result, the self-avoiding statistics is manifested in the force– D relation: $f(D) \approx D^{-8/3}$ [$\mathcal{F}(D) \approx D^{-5/3}$].

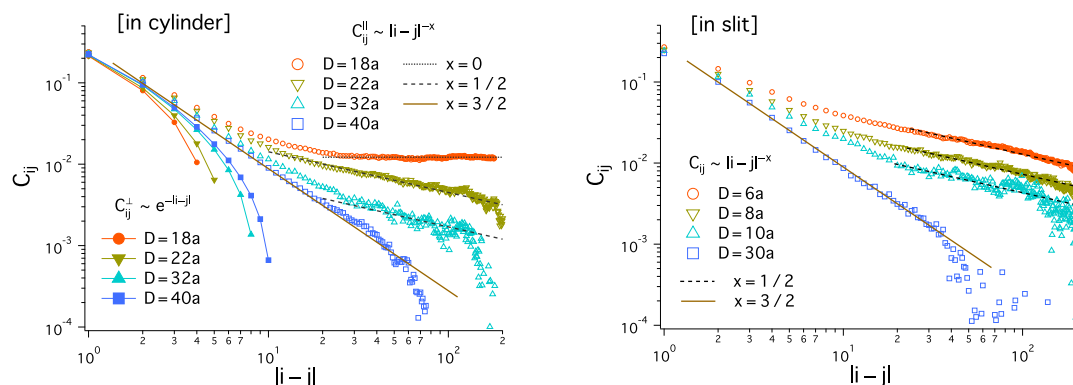


Figure 5. Bond–bond correlation function C_{ij} for a near- Θ polymer chain trapped in a cylindrical (left) or slit-like space (right). We have chosen $B_2 \approx 0.00202a^3$ ($\xi_T \approx 250a$ and $N_T = 62, 500$) and $N = 1000$ and used various values of $D = 18a, 22a, 32a, 40a$; in the slit case, D is a slit gap. The longitudinal component of the correlation function C_{ij}^{\parallel} is long ranged: $C_{ij}^{\parallel} \approx |i - j|^{-3/2}$ for the largest D value used, as for a Θ chain in the bulk (see the blue squares). For smaller D values, the effect of confinement is obvious: in both cases (left and right), enhanced self-avoidance tends to make the correlation “curves” more flat in a large $|i - j|$ range: $C_{ij}^{\parallel} \approx |i - j|^{-1/2}$ for $D = 22a, 32a$ (left) and for $D = 6a, 8a, 10a$ (right). The emergence of $C_{ij}^{\parallel} \approx |i - j|^0$ for small D ($D = 18a$) is unique to the cylindrical confinement and originates from the linear ordering of the chain (for larger values of D , linear ordering is not obvious, as indicated in Figure 3). In the graphs, the straight lines with various slopes (i.e., $-3/2$, $-1/2$, or 0) are to guide the eye. The regime characteristic of a “true” self-avoiding polymer with exponent β in eq 10 is, however, not realized with the parameters used. In contrast, the bond–bond correlation function in the transverse direction under cylindrical confinement $C_{ij}^{\perp}(|i - j|)$ decays exponentially for all D values used. A collision of monomers with the cylinder wall tends to randomize the correlation.

The diagram in Figure 4C shows the organization of a confined polymer in a D - B_2 plane. The chain breaks up into a linear string of possibly overlapping compression blobs of size $\approx D$ each (circles in cyan). The degree of overlapping is controlled by the size of thermal blobs (red circles): ξ_T . The larger D/ξ_T , the more strongly they repel each other. For sufficiently large D/ξ_T , the compression blobs become linearly arranged without overlapping. Also note that for the same B_2 , ξ_T is smaller for smaller D , because of enhanced self-avoidance. While the lower two cylinders fall in the extended de Gennes regime, the upper two belong to the de Gennes regime.

So far, we have focused on chain conformations and confinement free energy. To further advance our understanding of confinement effects on chain statistics, we have also examined bond–bond correlations, or the correlation between bond vectors \mathbf{u}_i and \mathbf{u}_j , where \mathbf{u}_i is a vector drawn from monomer i to monomer $i + 1$: $C_{ij} = \langle \mathbf{u}_i \cdot \mathbf{u}_j \rangle / a^2$. It has been known that C_{ij} is influenced by chain connectivity, self-avoidance, and confinement.^{19–22} It is thus useful to examine this quantity and relate it to the results in Figures 2–4.

A characteristic of “non-ideal” polymers is that their bond–bond correlation, C_{ij} , is long ranged and deviates from ideality under a variety of conditions (e.g., in a melt, in a Θ solvent, and under tube confinement).^{19–22} Of particular interest is the correlation for a single chain with weak self-avoidance,¹⁹ as is the case for $|i - j| < N_T \approx (\xi_T/a)^2$: in a free space, it can be expressed in our notations as

$$C_{ij} \approx B_2 |i - j|^{-1/2} + C |i - j|^{-3/2} \quad (9)$$

where C is a constant. For the case $|i - j| \ll N$, a similar result was obtained for a polymer melt;²¹ if the inequality is not satisfied, however, C_{ij} experiences finite-size effects and develops a more complex dependence on $|i - j|$.²¹ Outside this range, that is, $N_T \ll |i - j| \ll N$, the correlation becomes

$$C_{ij} \approx |i - j|^{-\beta} \quad (10)$$

where $\beta = 2 - 2\nu_F = 0.8$ (or more accurately, $\beta = 2 - 2 \times 0.588 \approx 0.824$);^{20,21} the exponent β here is to ensure that the bond–

bond correlation is consistent with the expected $R_g \approx aN^\nu$ for the case $R_g \gg \xi_T$, which is equivalent to $N \gg N_T$.¹

A systematic analysis of C_{ij} would necessitate a consideration of long chains with a varying degree of confinement. Here, our motivation is to show if confinement changes the exponent of C_{ij} in the way expected from the results in Figures 3 and 4. Our effort here is focused on the “obvious” effects of confinement on C_{ij} . To this end, we consider a near- Θ polymer under confinement and compare our simulation data against the correlations in eqs 9 and 10. While our primary focus is on cylindrical confinement, we also consider the slit-like confinement for comparison purposes.

Figure 5 shows in a log–log plot our results for C_{ij} obtained for a near- Θ chain in a cylindrical (left) and slit-like space (right). If C_{ij}^{\parallel} is the longitudinal component, C_{ij}^{\perp} is the transverse component. We have chosen $B_2 \approx 0.00202a^3$ and $N = 1000$ (as in Figures 2 and 4) as well as various values of the cylinder diameter or slit gap: $D = 18a, 22a, 32a, 40a$ (left) or $D = 6a, 8a, 10a, 30a$ (right). Recall that $\xi_T \approx 250a$ and $N_T = 62, 500$ for this choice of B_2 . To obtain reliable statistics and to minimize the “chain-end effect,” we averaged $C_{ij} = \langle \mathbf{u}_i \cdot \mathbf{u}_j \rangle / a^2$ over selected choices of i . Let i_{CM} be a monomer at the center of mass of the polymer; i is chosen to be in the range $i_{CM} \pm 5$. The correlation C_{ij} is averaged over all allowed values of i as well as over the simulation times.

As shown in Figure 5, the C_{ij} data for the largest D value (blue squares) tend to follow a simple power-law decay $C_{ij}^{\parallel} \approx |i - j|^{-3/2}$ for $|i - j| \lesssim 30$, as expected for a near- Θ polymer (see eq 9) (note that $D = 40a$; the largest value of D used for the cylindrically confined case is somewhat larger than $2R_g \approx 2 \times 17.5a = 35a$ for $N = 1000$). This scaling behavior was also observed for three-dimensional dense polymer solutions in the long-chain limit, in which individual chains behave like Θ chains.²¹

Confinement effects are, however, well reflected for small D values in the sense that C_{ij} decays more slowly, as is the case for $D \leq 32a$ and $D \leq 10a$ under cylindrical and slit confinement, respectively (see Figure 5). This is generally consistent with the finding that confinement enhances the self-avoidance of near- Θ polymers, as shown in Figure 3 and in earlier studies.⁴

Obviously, the scaling regime described by eq 10 is absent in Figure 5. In the bulk, this regime is realized if $N \gg N_T$.

As shown in the left graph in Figure 5, under cylindrical confinement, the C_{ij} exponent for an intermediate D range (i.e., for $D = 22a, 32a$) is close to $-3/2$ for a small range of $li - jl$ (bulk-like as for $D = 40a$) and approaches $-1/2$ in a large $li - jl$ range. This observation appears to be consistent with the scaling relation in eq 9, even though it is not so conclusive, because of the relatively narrow range of $li - jl$ shown in the graph. Along this line, it is worth noting that a similar crossover from the bulk-like to confined regimes was observed for a polymer melt under tube confinement.²² This points to the significance of confinement, similar to what the results in Figure 5 suggest. For $D = 18a$, $C_{ij}^{\parallel} \approx li - jl^0$ for $li - jl \gtrsim 20$, which is reminiscent of linear ordering (see Figure 3). In the linear-ordering regime, C_{ij} should not change with $li - jl$, as is most obvious for $D \approx a$. The main effect of partial randomization within a compression blob is to reduce the amplitude of C_{ij} , not the exponent.

The bond–bond correlation function in the transverse direction C_{ij}^{\perp} , however, decays exponentially for all values of D used. In a free space, both transverse and longitudinal components should decay in a similar fashion. The exponential decay of C_{ij}^{\perp} suggests that it feels cylinder wall effects, which tend to wash out any correction between bond vectors. In a random walk analogy, imagine a one-dimensional random walk with a directional correlation. Upon hitting a wall, it loses its directional memory. This appears to dominate the dependence of C_{ij}^{\perp} on $li - jl$. For a small $li - jl$ range, the wall effect should be minor. In this case, however, simulation details come into play, which will obscure the correct interpretation of the simulation data.

In slit geometry, as shown on the right in Figure 5, confinement effects are felt more slowly. In contrast to the cylindrically confined case on the left, confinement effects are not reflected when $D = 30a$. For smaller D values, that is, $D = 6a, 8a, 10a$, however, these effects change the exponent of C_{ij} from $-3/2$ to a less-negative value close to $-1/2$ in a large $li - jl$ range, similar to what is seen in the cylindrically confined case on the left in Figure 5. Obviously, the linear regime, where C_{ij} is constant, and the self-avoiding regime in eq 10 are not realized.

Finally, in both cases in Figure 5, the chain-end effect on C_{ij} appears to be more pronounced for a large D value. This can be understood as follows. When D is large, there are more monomers near the chain ends: the leftmost and rightmost monomers. This explains why the chain-end effect starts to be felt for a smaller $li - jl$ value, if D is larger, as indicated in Figure 5.

The results in Figures 3–5 complement each other. Our earlier interpretation of confinement effects in Figures 3 and 4 is consistent with what the results in Figure 5 suggest: confinement enhances the self-avoidance of near- Θ polymers.

CONCLUSIONS

In summary, we have shown how cylindrical confinement enhances the self-avoidance of near- Θ polymers: the stronger the confinement is, the stronger the self-avoidance is. While this general picture is well aligned with the recent studies with Θ polymers confined between two parallel plates or in slit confinement,⁴ it also has distinguishing features. The emergence of the so-called extended de Gennes regime is a good example.^{6–10} Also, three-body interactions are more relevant in low dimensions than in high dimensions; in three dimensions, they give rise to a logarithmic correction to chain sizes.^{3,4} In a confined Θ solvent (i.e., $B_2^{\text{cyl}} = 0$), these interactions are responsible for the linear organization of a confined polymer. As

pointed out,⁴ this condition is a singular point for single polymers; the solvent quality should be fine-tuned until the excluded volume vanishes exactly. As D changes, however, the polymer will shift from the confined- Θ point. As a result, the chain size scales as $R_{\parallel} \approx Na(D/a - 1)^{-4/3}$ in the large N limit, which deviates from $R_{\parallel} \approx Na(D/a)^{-1}$, as suggested from the conventional picture,⁵ in which $B_2 = 0$ independent of D .

In contrast to what we have observed with R_{\parallel} , the confinement free energy of near- Θ polymers is rather consistent with the earlier view of compression blobs as free-energy units.^{1,10} Inside each compression blob of size comparable to D , self-avoidance is insignificant, since it is smaller than the thermal blob.^{1,10} This is well aligned with the finding that the transverse component of internal distances resembles that of an ideal chain. Upon strong confinement ($D \ll R_g$), near- Θ polymers enter the extended de Gennes regime.^{6–10}

Finally, confinement-induced self-avoidance is well reflected in the bond–bond correlations, C_{ij} , of single near- Θ polymers, that is, $R_g \lesssim \xi_T$ or $N \lesssim N_T$. For a large value of D or in the bulk, C_{ij} follows a simple power-law decay: $C_{ij} \approx li - jl^{-3/2}$. Under cylindrical and slit-like confinement, the curves describing C_{ij} in a log–log plot become more flat in a large $li - jl$ range, as if self-avoidance is enhanced.

APPENDIX

In this appendix, we present a few steps that lead to the scaling form

$$B_2^{\text{cyl}} \approx \frac{a^3(D/a)^2}{(D/a - 1)^4} \quad (11)$$

which is introduced in the main text above eq 7. For this, we essentially follow recent studies.²³ Consider spherical particles of size a each, confined to the interior of a cylindrical space of length L and diameter D . The volume of the interior is $V = \pi(D/2)^2L$. Let $U(r)$ be the pair potential between two spheres at distance r apart and $E(r)$ the interaction between a sphere and the wall (in a numerically oriented approach, the cylinder wall can be viewed as being made of spherical particles. When a particle approaches the wall, it interacts with an “image” particle.²⁴ The details of this, however, will turn out to be irrelevant). The second virial coefficient of the resulting system is given as integrals with respect to the positions of two particles, that is, \mathbf{r}_1 and \mathbf{r}_2 , over the entire volume V ²³

$$-\frac{2}{V}B_2^{\text{cyl}}(D) = \frac{\int d\mathbf{r}_1 g(\mathbf{r}_1) \int d\mathbf{r}_2 g(\mathbf{r}_2) (e^{-U(r_{12})/k_B T} - 1)}{\int d\mathbf{r}_1 g(\mathbf{r}_1) \int d\mathbf{r}_2 g(\mathbf{r}_2)} \quad (12)$$

Here, $g(\mathbf{r}) = e^{-E(r)/k_B T}$ is to reflect the sphere and wall interaction, and $V' \equiv \int d\mathbf{r} g(\mathbf{r}) = \pi[(D - a)/2]^2L$ is the volume accessible to a sphere.

It proves useful to introduce the following integral

$$\Omega(D, \mathbf{r}_1) = g(\mathbf{r}_1) \int d\mathbf{r}_2 g(\mathbf{r}_2) (1 - e^{-U(r_{12})/k_B T}) \quad (13)$$

This is the excluded volume around a sphere at \mathbf{r}_1 that is inaccessible to other spheres in the system. If combined with eq 13, eq 12 becomes

$$\begin{aligned}
 B_2^{\text{cyl}}(D) &= \frac{V}{2(V')^2} \int \mathrm{d}\mathbf{r} \Omega(D, \mathbf{r}) \\
 &= \frac{2\pi LV}{2(V')^2} \int \mathrm{d}r_{\perp} r_{\perp} \Omega(D, r_{\perp}) \\
 &= \frac{4a^3(D/a)^2}{(D/a-1)^4} \times \frac{1}{a^5} \int \mathrm{d}r_{\perp} r_{\perp} \Omega(D, r_{\perp}) \quad (14)
 \end{aligned}$$

where r_{\perp} is the component of \mathbf{r} in the radial direction perpendicular to the long symmetry axis of the cylinder and the underlined term is dimensionless.

The underlined term in eq 14 is involved. Fortunately, for the case $D > 2a$, it can be dramatically simplified. To see this, note that $B_2^{\text{cyl}}(D)$ should reduce to the D -independent bulk value in the limit $D/a \gg 1$. The D -dependence of the underlined term will be different for different forms of $U(r)$, for example, hard spheres versus LJ particles. In this limit, for hard spheres, $B_2^{\text{cyl}}(D) \rightarrow B_2 = (2\pi/3)a^3$. This determines the D -dependence of the underlined term and thus that of $B_2^{\text{cyl}}(D)$ in eq 14

$$B_2^{\text{cyl}}(D) \approx \frac{4a^3(D/a)^2}{(D/a-1)^4} \times \left[\frac{\pi}{6} \left(\frac{D}{a} \right)^2 \right] \quad (15)$$

The term inside [...] approximates the underlined term in eq 14.

In contrast to the hard sphere case, for LJ particles in a bulk- Θ solvent, we expect $B_2(D \rightarrow \infty) \rightarrow 0$. This line of reasoning leads to

$$B_2^{\text{cyl}}(D) \approx \frac{4a^3(D/a)^2}{(D/a-1)^4} \times O(1) \quad (16)$$

This consideration will not fix the multiplicative prefactor. It is this D -dependence that we used for $B_2^{\text{cyl}}(D)$ in eq 7, which remains valid as long as $D > 2a$. A similar behavior was reported for a Θ chain in slit geometry.⁴

AUTHOR INFORMATION

Corresponding Authors

Youngkyun Jung – Supercomputing Center, Korea Institute of Science and Technology Information, Daejeon 34141, Korea; Email: yjung@kisti.re.kr

Changbong Hyeon – Korea Institute for Advanced Study, Seoul 02455, Korea; orcid.org/0000-0002-4844-7237; Email: hyeoncb@kias.re.kr

Bae-Yeun Ha – Department of Physics and Astronomy, University of Waterloo, Waterloo, Ontario N2L 3G1, Canada; Korea Institute for Advanced Study, Seoul 02455, Korea; orcid.org/0000-0003-2089-6759; Email: byha@uwaterloo.ca

Complete contact information is available at: <https://pubs.acs.org/10.1021/acs.macromol.9b02370>

Notes

The authors declare no competing financial interest.

ACKNOWLEDGMENTS

This work was supported by the Natural Sciences and Engineering Research Council of Canada (B.-Y.H.), a KIAS Individual Grant (CG035003) at Korea Institute for Advanced Study (C.H.), the National Research Foundation grant (NRF-2018R1D1A1B07051306; Y.J.), and the National Supercomputing Center (KSC-2019-CRE-0067).

REFERENCES

- (1) de Gennes, P.-G. *Scaling Concepts in Polymer Physics*; Cornell University Press, 1979.
- (2) Doi, M.; Edwards, S. F. *The Theory of Polymer Dynamics*; Oxford University Press, 1988.
- (3) Duplantier, B. Geometry of polymer chains near the theta-point and dimensional regularization. *J. Chem. Phys.* **1987**, *86*, 4233–4244.
- (4) Liu, L.; Pincus, P. A.; Hyeon, C. Compressing Θ -Chain in Slit Geometry. *Nano Lett.* **2019**, *19*, 5667–5673.
- (5) Raphael, E.; Pincus, P. Scaling theory of polymer solutions trapped in small pores: the Θ -solvent case. *J. Phys. II France* **1992**, *2*, 1341–1344.
- (6) Reisner, W.; Pedersen, J. N.; Austin, R. H. DNA confinement in nanochannels: physics and biological applications. *Rep. Prog. Phys.* **2012**, *75*, 106601.
- (7) Wang, Y.; Tree, D. R.; Dorfman, K. D. Simulation of DNA Extension in Nanochannels. *Macromolecules* **2011**, *44*, 6594–6604.
- (8) Dai, L.; van der Maarel, J.; Doyle, P. S. Extended de Gennes Regime of DNA Confined in a Nanochannel. *Macromolecules* **2014**, *47*, 2445–2450.
- (9) Dai, L.; Doyle, P. S. Comparisons of a Polymer in Confinement versus Applied Force. *Macromolecules* **2013**, *46*, 6336–6344.
- (10) Ha, B.-Y.; Jung, Y. Polymers under confinement: single polymers, how they interact, and as model chromosomes. *Soft Matter* **2015**, *11*, 2333–2352.
- (11) Wu, C.; Li, L. Unified description of transportation of polymer chains with different topologies through a small cylindrical pore. *Polymer* **2013**, *54*, 1463–1465.
- (12) Ge, H.; Wu, C. Separation of Linear and Star Chains by a Nanopore. *Macromolecules* **2010**, *43*, 8711–8713.
- (13) Kremer, K.; Grest, G. S. Dynamics of entangled linear polymer melts: A molecular-dynamics simulation. *J. Chem. Phys.* **1990**, *92*, 5057–5086.
- (14) Grest, G. S.; Kremer, K. Molecular dynamics simulation for polymers in the presence of a heat bath. *Phys. Rev. A* **1986**, *33*, 3628–3631.
- (15) Allen, M. P.; Tildesley, D. J. *Computer Simulation of Liquids*; Clarendon Press, 1987.
- (16) Frenkel, D.; Smit, B. *Understanding Molecular Simulation*; Academic Press, 2002.
- (17) Plimpton, S. Fast parallel algorithms for short-range molecular dynamics. *J. Comput. Phys.* **1995**, *117*, 1–19. Also see <http://lammps.sandia.gov>
- (18) Jun, S.; Thirumalai, D.; Ha, B.-Y. Compression and stretching of a self-avoiding chain in cylindrical nanopores. *Phys. Rev. Lett.* **2008**, *101*, 138101.
- (19) Shirvanyants, D.; Panyukov, S.; Liao, Q.; Rubinstein, M. Long-range correlations in a polymer chain due to its connectivity. *Macromolecules* **2008**, *41*, 1475–1485.
- (20) Hsu, H.-P.; Paul, W.; Binder, K. Polymer chain stiffness vs. excluded volume: A Monte Carlo study of the crossover towards the worm-like chain model. *Europhys. Lett.* **2010**, *92*, 28003.
- (21) Wittmer, J. P.; Meyer, H.; Baschnagel, J.; Johner, A.; Obukhov, S.; Mattioni, L.; Müller, M.; Semenov, A. N. Long range bond-bond correlations in dense polymer solutions. *Phys. Rev. Lett.* **2004**, *93*, 147801.
- (22) Lee, N.-K.; Farago, J.; Meyer, H.; Wittmer, J. P.; Baschnagel, J.; Obukhov, S. P.; Johner, A. Non-ideality of polymer melts confined to nanotubes. *Europhys. Lett.* **2011**, *93*, 48002.
- (23) Krekberg, W. P.; Mahynski, N. A.; Shen, V. K. On the virial coefficients of confined fluids: Analytic expressions for the thermodynamic properties of hard particles with attractions in slit and cylindrical pores to second order. *J. Chem. Phys.* **2019**, *150*, 044704.
- (24) Jeon, C.; Jung, Y.; Ha, B.-Y. Effects of molecular crowding and confinement on the spatial organization of a biopolymer. *Soft Matter* **2016**, *12*, 9436–9450.